Noninvasive Imaging of Inflammation by Ultrasound Detection of Phagocytosed Microbubbles

Jonathan R. Lindner, MD; Paul A. Dayton, ME; Matthew P. Coggins, BA; Klaus Ley, MD;
Ji Song, PhD; Katherine Ferrara, PhD; Sanjiv Kaul, MD

Background—We have previously shown that microbubbles adhere to leukocytes in regions of inflammation. We hypothesized that these microbubbles are phagocytosed by neutrophils and monocytes and remain acoustically active, permitting their detection in inflamed tissue.

Methods and Results—In vitro studies were performed in which activated leukocytes were incubated with albumin or lipid microbubbles and observed under microscopy. Microbubbles attached to the surface of activated neutrophils and monocytes, were phagocytosed, and remained intact for up to 30 minutes. The rate of destruction of the phagocytosed microbubbles on exposure to ultrasound was less ($P \leq 0.05$) than that of free microbubbles at all acoustic pressures applied. Intravital microscopy and simultaneous ultrasound imaging of the cremaster muscle was performed in 6 mice to determine whether phagocytosed microbubbles could be detected in vivo. Fifteen minutes after intravenous injection of fluorescein-labeled microbubbles, when the blood-pool concentration was negligible, the number of phagocytosed/attached microbubbles within venules was 7-fold greater in tumor necrosis factor-α (TNF-α)–treated animals than in control animals ($P < 0.01$). This increase in retained microbubbles resulted in a 5- to 6-fold-greater ($P < 0.01$) degree of ultrasound contrast enhancement than in controls.

Conclusions—After attaching to activated neutrophils and monocytes, microbubbles are phagocytosed intact. Despite viscoelastic damping, phagocytosed microbubbles remain responsive to ultrasound and can be detected by ultrasound in vivo after clearance of freely circulating microbubbles from the blood pool. Thus, contrast ultrasound has potential for imaging sites of inflammation. (***Circulation***. 2000;102:531-538.)

Key Words: imaging ∎ inflammation ∎ ultrasonics ∎ leukocytes

W e have recently demonstrated that microbubbles attach to activated leukocytes that are adherent to the endothelium of postcapillary venules after ischemia-reperfusion and during tumor necrosis factor-α (TNF-α)–induced inflammation.[1] The extent of microbubble attachment correlates with the degree of inflammation.[1] This phenomenon is probably responsible for the prolonged myocardial opacification seen after the administration of microbubbles after myocardial ischemia and reperfusion.[2]

We have shown that microbubble binding to leukocytes is influenced by the composition of the microbubble shell. Microbubbles composed of albumin adhere primarily through the leukocyte β_2-integrin Mac-1 (CD11b/CD18), whereas lipid microbubbles adhere through opsonization by serum complement.[1] The cell types responsible for leukocyte-microbubble interaction and the fate of microbubbles after their attachment to activated leukocytes is unknown.

In this study, we hypothesized that microbubbles are phagocytosed by activated leukocytes that express Mac-1 and other complement receptors and remain acoustically active,

thereby permitting their detection at sites of inflammation. To investigate these hypotheses, in vitro studies were performed to determine the leukocyte cell types involved and to assess the responses of phagocytosed microbubbles to ultrasound (US). The feasibility of imaging these microbubbles in vivo was assessed by means of simultaneous intravital microscopy and US imaging of inflamed cremaster muscle in mice.

Methods

Microbubbles and Isolation of Leukocytes

Perfluorocarbon gas–filled microbubbles with shells composed of either albumin or lipid (Optison or MP1950, Mallinckrodt Medical) were used. Lipid microbubbles contained phosphatidylcholine, a surfactant, and a fluorescein derivative of phosphatidylethanolamine in a molar ratio of $\approx75:15:1$. The microbubble size ranged from 2.8 to 4.1 μm. Approximately 2×10^7 microbubbles were used for each in vitro experiment.

Leukocytes were isolated from whole blood collected from healthy volunteers. A portion of this blood was used to obtain serum and the remainder was anticoagulated with heparin (10 U/mL). Neutrophil and monocyte/lymphocyte fractions were isolated with

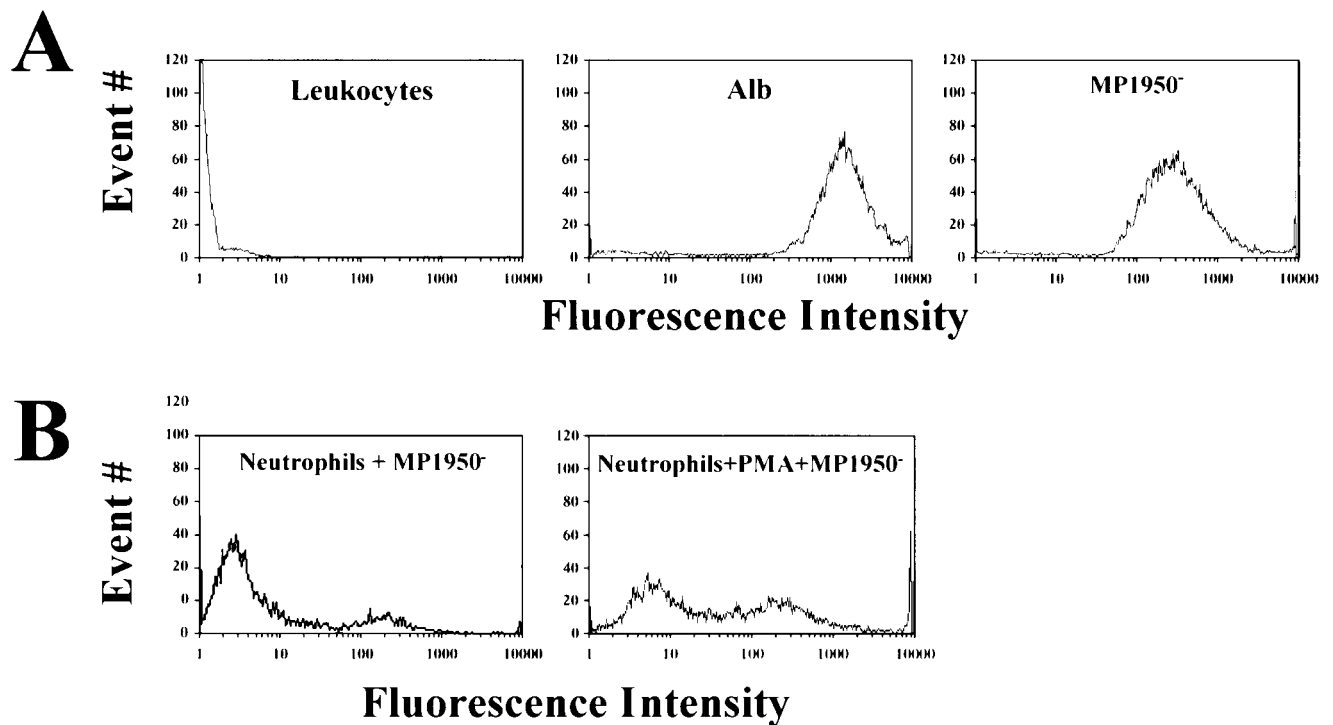*Circulation* **is available at http://www.circulationaha.org**

A

B

Figure 1. Examples of green fluorescence histograms obtained by flow cytometry of (A) leukocytes or microbubbles alone or (B) after incubation of lipid microbubbles with neutrophils (nonactivated and PMA-activated). See text for details.

Ficoll-Hypaque density gradient centrifugation (Mono-Poly, ICN Pharmaceuticals),[3] washed twice, and resuspended in PBS. Leukocyte concentrations were determined with hemocytometer measurements of Kimura-stained samples. For each in vivo experiment, 2×10^6 leukocytes were combined with 0.2 mL of serum and 0.2 mL of PBS containing 2 mmol/L $MgCl_2$ and $CaCl_2$. Leukocytes were activated by 10 nmol/L phorbol myristate acetate (PMA) 15 minutes before use.

Determination of Cell Types Responsible for Leukocyte-Microbubble Interactions

Flow cytometry was performed to determine the cell types involved in leukocyte-microbubble interactions. Activated or nonactivated leukocytes were combined with fluorescein-labeled albumin or lipid microbubbles and incubated during gentle agitation for 3 minutes at 37°C. Red blood cells were hypotonically lysed, and samples were analyzed with a flow cytometer (FACScan, Becton Dickinson). Separate analysis was performed for neutrophils, monocytes, and lymphocytes by gating according to their characteristic side and forward light-scatter patterns.[4] Gating also permitted exclusion of free microbubbles from analysis.[1] Experiments were performed in duplicate, and the data were displayed as histograms of green fluorescence in a gated population.

Temporal Characterization of Microbubble-Leukocyte Interactions

Microscopy was performed to determine the fate of microbubbles after their attachment to activated leukocytes. Samples (50 μL) were removed 3, 15, and 30 minutes after activated leukocytes were incubated with microbubbles, placed on a slide, and observed with an inverted microscope (Axiovert, Carl Zeiss) with an oil-immersion objective ($\times$100/1.3 numerical aperture). A minimum of 50 cells were identified under transillumination and classified according to whether they interacted (by attachment or phagocytosis) with microbubbles.

For transmission electron microscopy (TEM), samples (150 μL) from the leukocyte-microbubble suspensions were placed in an equivalent volume of 0.1 mol/L sodium cacodylate buffer (pH 7.5)

containing 2% osmium tetroxide for 30 minutes. They were centrifuged, washed in PBS, fixed in 2% glutaraldehyde/paraformaldehyde, dehydrated in a graded series of acetone, and embedded in epoxy resin. Thin sections were stained with saturated uranyl acetate and lead citrate. Observations were made at final magnification of $\times$6600 with a transmission electron microscope (100CX, Jeol).

Microbubble Responses to US

To evaluate the acoustic activity of phagocytosed microbubbles, we first performed in vitro studies by using a system that allowed simultaneous US exposure and light microscopy. A syringe containing microbubble-leukocyte suspensions was connected to a 4- to 6-cm segment of cellulose tubing with an internal diameter of 200 μm. This tubing was immersed in a water bath secured to the stage of a light microscope (IV500L, Mikron Instruments) and positioned in the focal planes of a water immersion objective (SW 100/1.3 numerical aperture) and a 2.25-MHz, spherically focused US transducer (V306, Panametrics) oriented perpendicular to each other. The transducer was interfaced to a square-wave pulse generator (SP-801A, Ritec) to produce broad-band pulses of $\approx$1.5 cycles at the center frequency. Acoustic pressure measurements were made at the focal plane before each experiment with a calibrated needle hydrophone (PZT 2422-0200, Specialty Engineering Associates).

Activated leukocyte and microbubble suspensions were placed in a microinjector (IM-5B, Narishige) that allowed positioning of a single cell or microbubble in the optical field. Free and phagocytosed microbubbles were repeatedly exposed to single pulses of US with peak negative acoustic pressures of -400, -940, or -1600 kPa. Recordings were made with a video camera (Motioncorder 1000, Kodak) interfaced with an S-VHS recorder (AG-1980, Panasonic).

Microbubble diameters were measured off-line with video calipers, and microbubble volume was calculated assuming a spherical geometry. The rate of reduction in microbubble size during US pulsing was determined by fitting a monoexponential function, $y=e^{-\beta x}+C$, to the relation between pulse number and microbubble volume, where y is normalized microbubble volume, β is the time constant of the decay, and C is a constant.
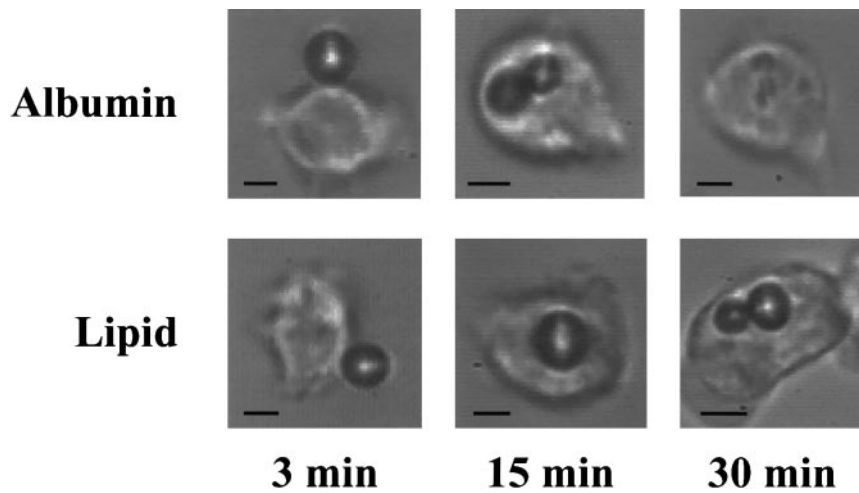
Figure 2. Images obtained on light microscopy illustrating microbubble attachment to surface of activated neutrophils at 3 minutes and phagocytosis of microbubbles by 15 minutes. At 30 minutes, only lipid microbubbles remained intact. Scale bars=2.5 μm.

In Vivo Detection of Phagocytosed Microbubbles

The study protocol was approved by the animal research committee at the University of Virginia. Six male wild-type C57BL/6 mice (22 to 30 g) were anesthetized with an intraperitoneal injection of a solution containing ketamine hydrochloride, xylazine, and atropine. Body temperature was maintained at 37°C with a heating pad. Both jugular veins were cannulated for administration of microbubbles and drugs. Anesthesia was maintained with intravenous administration of 0.1 mg pentobarbital every 45 minutes as needed. A cremaster muscle was prepared for intravital microscopy.[5] The muscle was exteriorized through a scrotal incision and secured to a translucent pedestal. A longitudinal incision was made in the muscle, and the edges were secured to the pedestal. The preparation was superfused continuously with isothermic bicarbonate-buffered saline.

Microscopic observations were made with an intravital microscope (Axioskop 2 FS, Carl Zeiss, Inc) with a saline immersion objective (SW 40/0.8 numerical aperture). Epifluorescent imaging was performed with an excitation filter for fluorescein (460 to 500 nm). Video recordings were made with a high-resolution CCD camera (C2400, Hamamatsu Photonics) connected to an S-VHS recorder (S9500, JVC).

Centerline venular red blood cell velocities were measured with a dual-slit photodiode[6] (CircuSoft Instrumentation) and converted to mean velocities by multiplying by 0.625.[7] Shear rates (γ_w) were determined by means of the equation $\gamma_w=2.12(8V_b)/d$, where V_b is the mean blood velocity, d is the vessel diameter measured off-line with video-calipers, and 2.12 is a correction factor for the velocity profile.[8] Adherent leukocytes, defined as those not moving for ≥ 30 seconds, were counted and expressed per venular surface area, calculated from offline diameter and length measurements.

US was performed with a Sonos 5500 system (Agilent Technologies) with harmonic imaging at transmit and receive frequencies of 1.8 and 3.6 MHz, respectively. The US transducer was placed in a bath containing isothermic bicarbonate-buffered saline surrounding the pedestal and positioned perpendicular to the microscope objective. A mechanical index of 0.9 and a compression of 75% were used. Gain was optimized at the beginning of each experiment and was held constant. The US pulsing interval (PI) was controlled with an internal timer. Video recordings were made with an S-VHS recorder (MD-830, Panasonic).

Inflammation of the cremaster was produced in 3 mice by intrascrotal injection of 0.5 μg of murine recombinant TNF-α (Sigma) in 0.2 mL saline 2 hours before dissection, and 3 mice
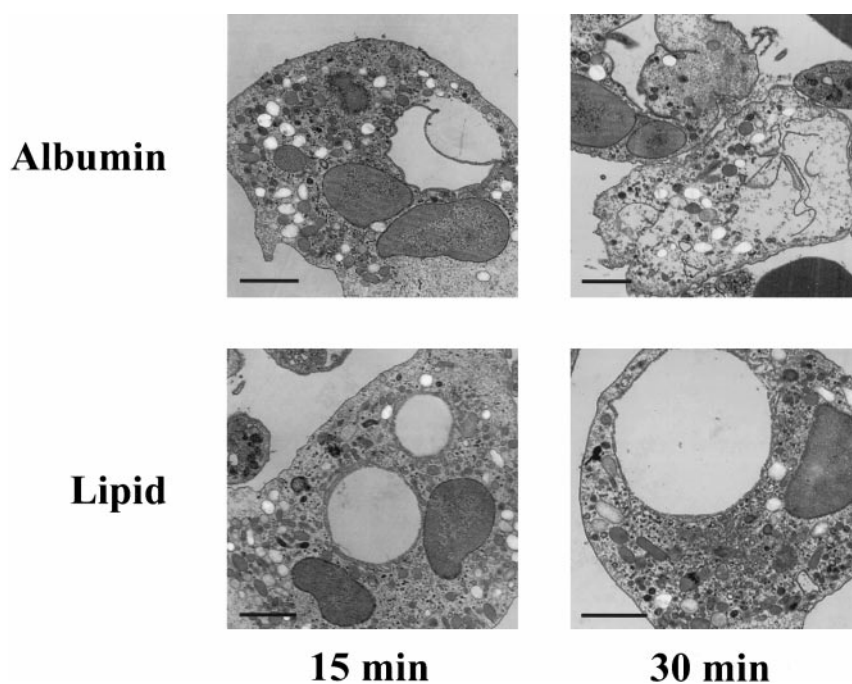

Figure 3. Images obtained by TEM confirming phagocytosis of microbubbles by activated neutrophils. Separation of albumin shell from surrounding cytoplasm in image at 15 minutes was due to partial deflation of microbubble during fixation. At 30 minutes, lipid microbubbles remained intact, whereas albumin microbubbles were degraded into shell fragments and intracellular gas. Scale bars=2 μm.
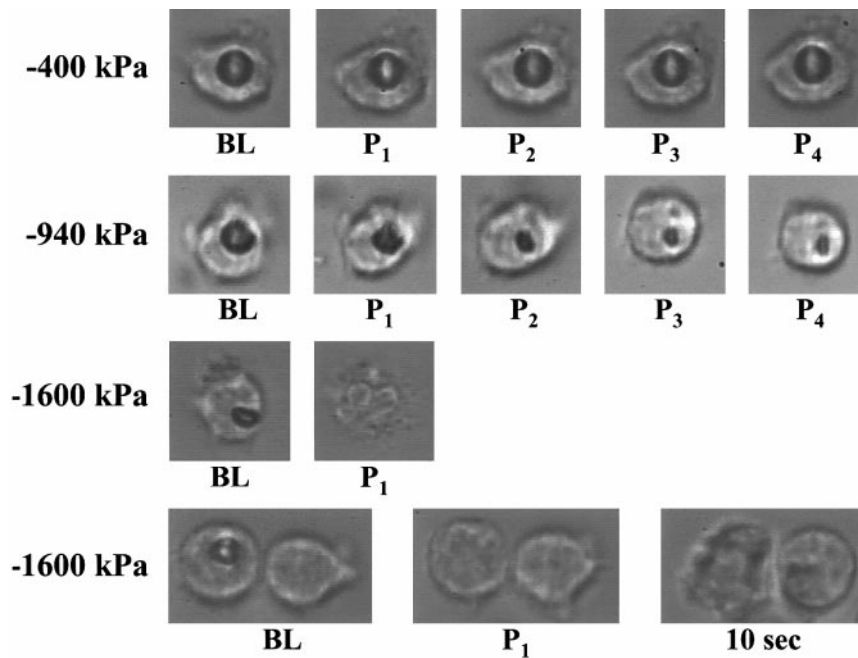
Figure 4. Images obtained on light microscopy illustrating effect of single pulses of US (P_1 through P_4) at peak negative acoustic pressures of -400, -940, and -1600 kPa on phagocytosed albumin microbubbles. Examples of neutrophil cell membrane disruption and distortion at -1600 kPa are shown. See text for details. BL indicates baseline.

served as controls. Observations were made in venules with diameters between 25 and 40 μm. To assess venular hemodynamics and the degree of leukocyte adhesion, 3 venules were recorded under transillumination followed by measurement of centerline blood velocity. Immediately after intravenous injection of 2×10^7 fluorescein-labeled microbubbles, 20 separate high-power fields encompassing the venules were observed over a period of 2 minutes with fluorescent epi-illumination. These observations were repeated 15 minutes after injection of microbubbles. Because of the potential of US to destroy microbubbles,[9,10] US examination was not performed at either of these 2 stages.

US imaging was initiated 17 minutes after microbubble injection, when the blood pool concentration of freely circulating microbubbles should be negligible. The video intensity (VI) in the first frame on resumption of US imaging should reflect the total tissue concentra-tion of microbubbles (adhered, phagocytosed, and freely circulating); that of the next frame should reflect microbubbles that have either not been destroyed or that have reentered the region from the circulating blood pool.[11] If the microbubble blood pool concentration is low, and if nearly all microbubbles are destroyed by the first US pulse, then the VI should be much lower in the second than in first pulse. Accordingly, on resumption of US imaging, a first set of 5 images was obtained at a PI of 0.5 seconds followed by a second set of 3 images at a PI of 30 seconds. The second set of images was obtained to assess the signal from freely circulating microbubbles, because microbubble replenishment into tissue should be complete 30 seconds after a US pulse.[11]

US images were analyzed offline as previously described.[12] Several precontrast frames (obtained before microbubble injection) were averaged to create a baseline image. This image was then
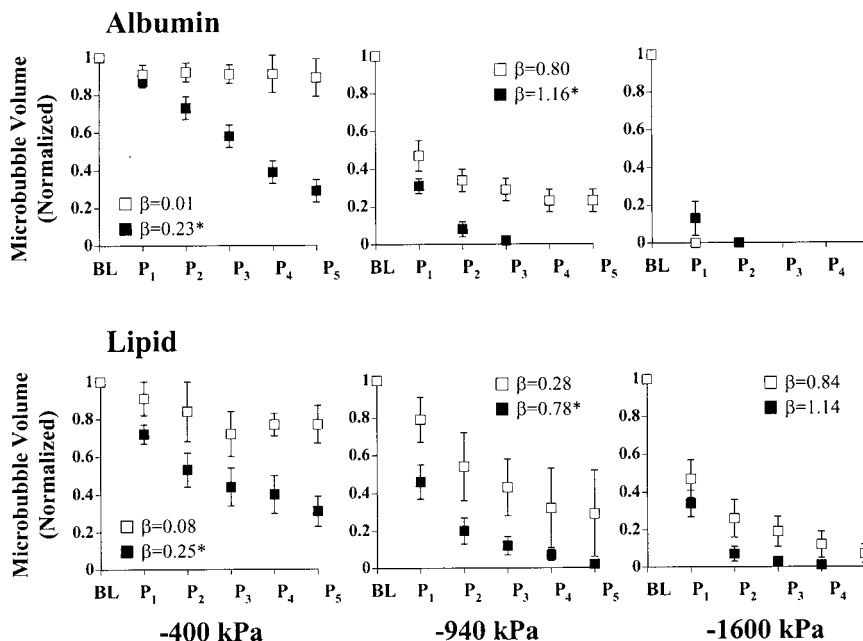

Figure 5. Mean ($\pm$SEM) normalized volumes of free (■) and phagocytosed (□) albumin and lipid microbubbles at baseline (BL) and after sequential pulses of US (P_1 through P_5) at peak negative acoustic pressures of -400, -940, and -1600 kPa. Rate constants (β) of decay of microbubble volume are shown. *$P<0.05$ vs free microbubbles.

TABLE 1. Venular Hemodynamic Parameters and Leukocyte Adhesion Data in Control and TNF-α–treated Mice

	Control	TNF-α
Venules, n	9	9
Venular diameter, μm	34.6±3.6	30.6±4.8
Blood velocity, μm · s^{-1}	1778±431	1906±378
Wall shear rate, s^{-1}	804±270	979±222
Leukocyte adherence, mm^{-2}	201±101	1546±210*

*$P<0.0001$ compared with TNF-α data.

subtracted from each of the images from the first set as well as a similarly averaged image from the second set.

Statistical Analysis

Data are expressed as mean±SD. Nominal comparisons were made by Fisher's exact test. Repeated-measures ANOVA was used to compare flow cytometry data and to determine differences in rate constants of microbubble decay in vivo. Comparisons of in vivo data were made by means of a Student's t test. Differences were considered significant at $P<0.05$ (2-sided).

Results

Cell Types Involved in Leukocyte-Microbubble Interactions

On flow cytometry, fluorescein-labeled microbubbles alone were intensely fluorescent, whereas leukocytes had little fluorescence (Figure 1A). Figure 1B shows examples of histograms obtained after lipid microbubbles were combined with neutrophils and free microbubbles were excluded from analysis by gating to light-scatter pattern. Microbubble attachment to neutrophils was indicated by the appearance of a fluorescent peak associated with these cells, which was greater when cells were activated by PMA. After activation, the proportion of neutrophils interacting with microbubbles increased from 0.15±0.03 to 0.47±0.05 ($P<0.05$) for lipid microbubbles and from 0.17±0.04 to 0.85±0.07 for albumin microbubbles ($P<0.05$). The proportion of monocytes interacting similarly increased from 0.16±0.04 to 0.60±0.05 ($P<0.05$) and from 0.06±0.01 to 0.12±0.02 ($P<0.05$) for albumin and lipid microbubbles, respectively.

Temporal Characterization of Leukocyte-Microbubble Interactions

The sequence of microbubble-leukocyte interactions over time is illustrated in Figure 2. Early (3 minutes after their combination), microbubbles attached to the cell surface of

Figure 6. Mean (±SD) number of microbubble-leukocyte interactions per 20 optical fields in control and TNF-α–treated mice. *$P<0.01$ vs corresponding data for control animals.

activated leukocytes, ranging from 1 to 6 microbubbles per leukocyte. Most of these microbubbles were phagocytosed intact by 15 minutes. By 30 minutes, however, intracellular albumin microbubbles were degraded into shell and bubble fragments, whereas lipid microbubbles remained intact. At all time points, the percentage of cells interacting with either microbubble type was less ($P<0.05$) for the lymphocyte-monocyte fraction than for neutrophils ($<10\%$ compared with $>50\%$ of cells).

Confirmation of the intracellular location of microbubbles was made with TEM (Figure 3), since microbubbles attached to leukocytes might assume a polar orientation on the cell surface as the result of buoyancy and therefore appear to be intracellular on light microscopy. At 30 minutes, albumin microbubble shells were significantly degraded with adjacent organelle paucity, consistent with intracellular retention of the perfluorocarbon gas (Figure 3). In comparison, lipid microbubbles remained intact at this time point.

Response of Phagocytosed Microbubbles to US

In the in vitro studies, the mean microbubble diameters before US exposure were not significantly different for free versus phagocytosed albumin (3.16±0.64 versus 2.94±0.62 μm) or lipid (3.42±1.06 versus 3.08±0.82 μm) microbubbles. Figure 4 depicts the effect of repetitive single pulses of US on the size of single phagocytosed albumin microbubbles viewed under light microscopy. At a low acoustic pressure (-400 kPa), each US pulse resulted in minimal change in microbubble size compared with baseline. At a moderate acoustic pressure (-940 kPa), individual pulses of US resulted in sequential reductions in microbubble size until destruction was complete. At a high acoustic pressure (-1600 kPa), albumin microbubbles were destroyed by a single US pulse. Microbubble destruction at this pressure frequently caused either distortion of the cell membrane within seconds of microbubble destruction or immediate rupture of the neutrophil cell membrane, indicated by collapse of the cell and efflux of its cytoplasmic granules into the surrounding medium. These effects were also observed with lipid microbubble destruction at -1600 kPa.

Figure 5 illustrates the rates of decline in microbubble volume with repetitive pulses of US at various peak negative acoustic pressures. Peak negative pressures of -400 kPa had little effect on phagocytosed microbubbles, regardless of their composition, but produced a gradual decline in volume of free microbubbles. At a peak negative pressure of -940 kPa, sequential US pulses resulted in incremental reductions in microbubble volumes of both free and phagocytosed microbubbles. At -1600 kPa, a single US pulse caused destruction of all albumin microbubbles, whereas lipid microbubble destruction required several pulses. Overall, increasing the acoustic pressure resulted in a greater ($P<0.05$) rate of decline in microbubble size, irrespective of shell composition or location (free versus intracellular). The rate of decay in size at each pressure was lower for the intracellular microbubbles. The only exception was lipid microbubbles exposed to -1600 kPa, in which the difference in the decay rates for the free and intracellular microbubbles was marginal ($P=0.05$). The time constants of decay at this pressure were
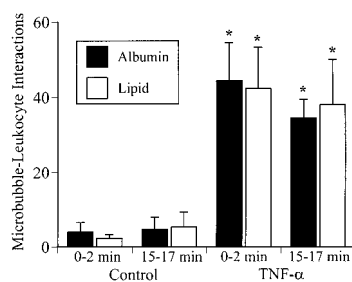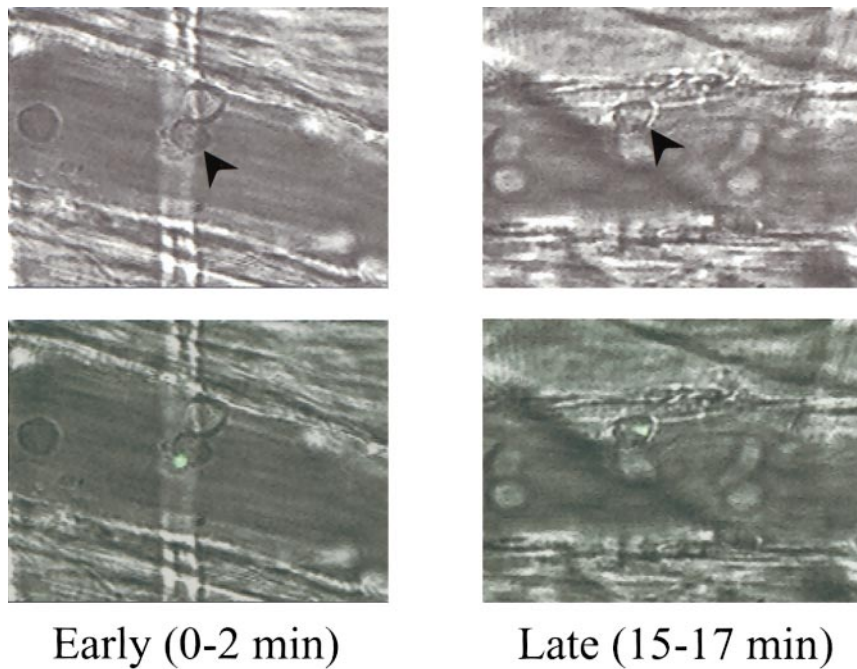
Early (0-2 min)　　Late (15-17 min)

Figure 7. Images of cremaster muscle from a TNF-α–treated mouse during transillumination (top) and fluorescent epi-illumination (bottom) of venular segments early (0 to 2 minutes) and late (15 to 17 minutes) after intravenous injections of fluorescein-labeled albumin microbubbles. Arrowheads indicate adhered leukocytes on transillumination that were observed to bind and phagocytose albumin microbubbles in corresponding fluorescent images.

not calculated for albumin microbubbles because of their complete destruction with the first US pulse.

In the in vivo experiments, the mean venular diameter, blood flow velocity, and shear rate were similar in control and TNF-α–treated mice (Table). The mean number of adherent leukocytes was >7-fold higher after TNF-α treatment than in controls (Table), indicating an intense inflammatory response.

In control mice, microbubble interactions with the few adherent leukocytes were uncommon when observations were made both early (0 to 2 minutes) and late (15 to 17 minutes) after their intravenous injection (Figure 6). In comparison, treatment with TNF-α resulted in a far greater number of microbubble interactions with the abundant adherent leukocytes at both time points. Microbubbles attached to the leukocyte surface early after injection, and most appeared to be phagocytosed by 15 to 17 minutes (Figure 7), at which time freely circulating microbubbles were only occasionally observed (<1 microbubble transiting the venules every 10 seconds). Unlike in the in vitro setting, no obvious disruption of the leukocyte membrane was observed when phagocytosed microbubbles were insonified.

Figure 8 illustrates examples of US images of the cremaster muscles in a control and a TNF-α–treated mouse. In the control animal, the VI increased minimally 17 minutes after lipid microbubble injection compared with baseline (precontrast) from the few freely circulating microbubbles passing through the tissue. In comparison, intense contrast enhancement was seen at this time in the TNF-α–treated mouse, which mostly represented signal from the phagocytosed/attached microbubbles retained at the site of inflammation. All microbubbles were destroyed by the initial pulse of US so that the VI in the next frame, obtained 0.5 second later, was reduced and resembled that of the baseline image. The VI increased minimally when the PI was prolonged to 30 seconds, which allowed complete replenishment of the tissue from circulating microbubbles. The VI in this frame was much less than that seen in the first frame obtained after microbubble injection in the TNF-α–treated animal, indicating that the signal from the few freely circulating microbubbles was very low.

The mean background-subtracted VI from the cremaster muscles of all mice is shown in Figure 9. In control mice, the
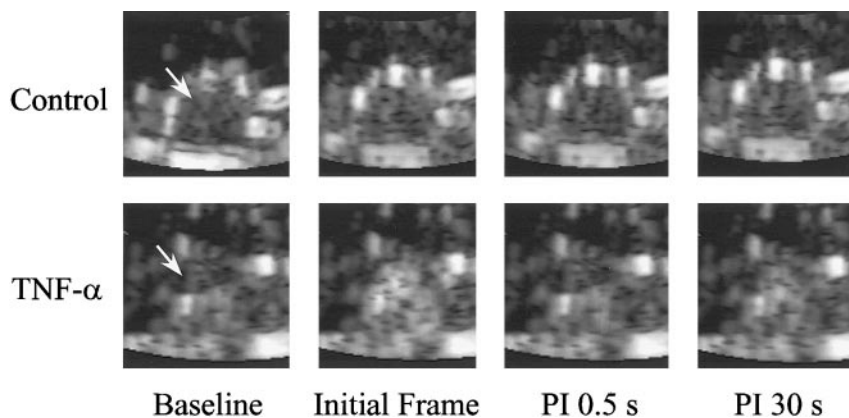

Baseline　　Initial Frame　　PI 0.5 s　　PI 30 s

Figure 8. US images of cremaster muscle (arrow) mounted on circular pedestal from control and TNF-α–treated mouse obtained before (baseline) and 17 minutes after lipid microbubble injection. Late images include initial frame obtained on resumption of imaging, next frame 0.5 second later, and frame subsequently obtained at PI of 30 seconds.
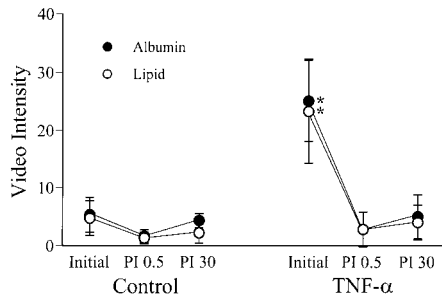
Figure 9. Mean (±SD) background-subtracted VI from cremaster muscles of control and TNF-α–treated mice from initial frames obtained on resumption of US imaging (Initial), frames obtained 0.5 second later (PI 0.5), and frames subsequently acquired at PI of 30 seconds. *$P<0.01$ vs data obtained at PI of 0.5 and 30 seconds.

VI was low in the initial frame obtained on resumption of imaging 17 minutes after injection of albumin or lipid microbubbles. Because of US-induced microbubble destruction, the VI decreased slightly on the next frame obtained 0.5 second later. The mean VI from subsequent images obtained at a PI of 30 seconds, which represented signal from freely circulating microbubbles, was not significantly different from the initial frame. The mean background-subtracted VI on the initial frame on resumption of imaging 17 minutes after microbubble injection was 5- to 6-fold greater ($P<0.01$) in TNF-α–treated compared with control animals. The VI on the next frame 0.5 second later was much lower as a result of microbubble destruction and increased only marginally at a PI of 30 seconds from tissue replenishment by freely circulating microbubbles. These results indicate that the intense signal noted on resumption of imaging 17 minutes after microbubble injection was due to phagocytosed or attached microbubbles retained within the inflamed tissue rather than those freely circulating in the blood pool.

Discussion

We have recently reported that microbubbles attach to activated leukocytes adherent to the venular endothelium after ischemia-reperfusion and TNF-α–induced inflammation.[1] The new information obtained from this study is that (1) neutrophils and monocytes are responsible for leukocyte-microbubble interactions; (2) after attachment, microbubbles are phagocytosed intact; and (3) despite viscoelastic damping, phagocytosed microbubbles remain acoustically active, thereby permitting their detection by US imaging of inflamed tissue. These results indicate that with microbubbles, it may be possible to noninvasively image inflammation in organ systems accessible to US and also conceivably administer drugs to these sites.

Characterization of Microbubble-Leukocyte Interactions

We have previously shown that microbubble-leukocyte interactions are influenced by the microbubble shell composition. Albumin microbubbles attach to leukocytes through the β_2-integrin Mac-1 on the surface of the activated leukocytes, whereas lipid microbubbles attach to activated leukocytes through opsonization by serum complement.[1] In this study,

we found that the cells involved were primarily neutrophils and monocytes, both of which express active Mac-1 and other complement receptors on cell activation.[13,14]

Although we have observed attachment of microbubbles in vivo to leukocytes adherent to inflamed venular endothelium,[1] the consequent fate of these microbubbles was not defined. In this study, we found that these microbubbles were phagocytosed intact within minutes by activated leukocytes. This finding is consistent with the specific role of Mac-1 and complement receptors in immunoglobulin-independent phagocytosis.[15]

Response of Phagocytosed Microbubbles to US

Currently, the detection of microbubbles in tissue depends on their nonlinear behavior in a US field as well as microbubble destruction that occurs when acoustic pressure is sufficiently high.[9,10] As illustrated in this and previous studies,[9] free microbubble destruction can occur with a single US pulse delivered at a high negative acoustic pressure. At more moderate acoustic pressures, the destruction is gradual, with progressive deflation of the microbubbles with each subsequent US pulse. Microbubble oscillation at moderate US pressures most likely results in less severe shell defects with partial release of gas into the surrounding medium or simply in augmented outward movement of gas during the compressive phase.[9]

The magnitude of US-mediated microbubble oscillations will depend on several factors, including the composition of the gas and shell as well as the degree of viscous and thermal damping.[16,17] It is probable that oscillations of the phagocytosed microbubbles in this study were damped by the viscoelastic properties of the surrounding cellular milieu, resulting in smaller fluctuations in size and less shell damage compared with free microbubbles. As a result, a lower rate of decline in size was found for phagocytosed compared with free microbubbles at moderate peak negative pressures (-400 and -940 kPa).

Because of differences in the material properties of their shells, albumin and lipid microbubbles behaved somewhat differently at the highest acoustic pressure applied in our experiments (-1600 kPa). At this pressure, albumin microbubbles were more susceptible to destruction than lipid microbubbles. Destruction of either occasionally caused disruption of the neutrophil cell membrane, probably caused by the large amplitude of microbubble oscillations at this pressure. Other potential mechanisms for this effect include local shock or thermal effects or membrane damage caused by outward shell fragmentation.[9] These detrimental effects on the leukocyte noted in vitro were not reproduced in vivo at acoustic pressures generated by US systems used clinically.

The change in microbubble size on US exposure in vitro indicated that despite viscoelastic damping, phagocytosed microbubbles were acoustically active. To determine whether phagocytosed microbubble signals could be detected in vivo, we imaged the cremaster muscle of mice in the presence of TNF-α–induced inflammation. The numbers of both the adherent leukocytes and the microbubbles interacting with them increased by $\approx$7-fold in TNF-α–treated animals. US imaging initiated >15 minutes after microbubble injection

(which allowed microbubble concentration in the blood pool to become negligible) revealed bright opacification of the cremaster on the initial frame only in the setting of inflammation. The assumption that this opacification resulted from microbubbles associated with adherent leukocytes was supported by the abundant phagocytosed microbubbles seen by intravital microscopy performed just before initiation of US. Only a few freely circulating microbubbles were seen and were responsible for a minimal change in VI at a PI of 30 seconds compared with baseline.

In conclusion, we have demonstrated that microbubbles are rapidly phagocytosed intact by activated neutrophils and monocytes and can persist intracellularly for almost half an hour before they are degraded. In this period, microbubbles remain acoustically active despite viscoelastic damping caused by the cellular milieu, thereby allowing their detection on US imaging. These findings indicate that contrast-enhanced US may provide a useful means for the noninvasive assessment of inflammation and to follow the response to treatment. Future studies are being directed at optimizing imaging protocols for detection of phagocytosed microbubbles and development of microbubbles with even greater avidity for leukocytes.

Acknowledgments

References

1. Lindner JR, Coggins MP, Kaul S, et al. Microbubble persistence in the microcirculation during ischemia/reperfusion and inflammation is caused by integrin- and complement-mediated adherence to activated leukocytes. *Circulation*. 2000;101:668–675.
2. Lindner JR, Ismail S, Spotnitz WD, et al. Albumin microbubble persistence during myocardial contrast echocardiography is associated with microvascular endothelial glycocalyx damage. *Circulation*. 1998;98:2187–2194.
3. Ferrante A, Thong YH. A rapid one-step procedure for purification of mononuclear and polymorphonuclear leukocytes from human blood using a modification of the Hypaque-Ficoll technique. *J Immunol Methods*. 1978;24:389–393.
4. Riley RS, Mahin EJ, Ross W, et al. Techniques of cellular analysis. In: Riley RS, ed. *Clinical Applications of Flow Cytometry*. New York, NY: Igaki-Shoin; 1993:195–250.
5. Ley K, Bullard DC, Arbones ML, et al. Sequential contribution of L- and P-selectin to leukocyte rolling in vivo. *J Exp Med*. 1995;181:669–675.
6. Pries AR. A versatile video image analysis system for microcirculatory research. *Int J Microcirc Clin Exp*. 1988;7:327–345.
7. Lipowski HH, Zweifach BW. Application of the "two-slit" photometric technique to the measurement of microvascular volumetric flow rates. *Microvasc Res*. 1978;15:93–101.
8. Reneman RS, Woldhuis B, oude Egbrink MGA, et al. Concentration and velocity profiles of blood cells in the microcirculation. In: Hwang NHC, Turitto VT, Yen MRT, eds. *Advances in Cardiovascular Engineering*. New York, NY: Plenum; 1992:25–40.
9. Dayton PA, Morgan KE, Klibanov AL, et al. Optical and acoustical observations of the effects of ultrasound on contrast agents. *IEEE Trans Ultrason Ferroelect Freq Contr*. 1999;46:220–232.
10. Wei K, Skyba DM, Firschke C, et al. Interaction between microbubbles and ultrasound: in vitro and in vivo observations. *J Am Coll Cardiol*. 1997;29:1081–1088.
11. Wei K, Jayaweera AR, Firoozan S, et al. Quantification of myocardial blood flow with ultrasound-induced destruction of microbubbles administered as a constant venous infusion. *Circulation*. 1998;97:473–483.
12. Jayaweera AR, Sklenar J, Kaul S. Quantification of images obtained during myocardial contrast echocardiography. *Echocardiography*. 1994;11:385–396.
13. Diamond MS, Springer TA. A subpopulation of Mac-1 (CD11b/CD18) molecules mediates neutrophil adhesion to ICAM-1 and fibrinogen. *J Cell Biol*. 1993;120:545–556.
14. Berger M, O'Shea J, Cross AS, et al. Human neutrophils increase expression of C3bi as well as C3b receptors upon activation. *J Clin Invest*. 1984;74:1566–1571.
15. Graham IL, Brown EJ. Extracellular calcium results in a conformational change in Mac-1 (CD11b/CD18) on neutrophils: differentiation of adhesion and phagocytosis functions of Mac-1. *J Immunol*. 1991;146:685–691.
16. Hoff L, Sontum PC, Hoff B. Acoustic properties of shell-encapsulated, gas-filled ultrasound contrast agents. *Proceedings of the 1996 IEEE Ultrasonics Symposium*. 1996;2:1441–1444.
17. de Jong N, Ten Cate FJ, Lancee CT, et al. Principles and recent developments in ultrasound contrast agents. *Ultrasonics*. 1991;29:324–330.